analytical chemistry

pubs.acs.org/ac

Article

Ultrasensitive Electrochemiluminescence Biosensor Using Sulfur Quantum Dots as an Emitter and an Efficient DNA Walking Machine with Triple-Stranded DNA as a Signal Amplifier

Linlei Liu, Yue Zhang, Ruo Yuan,* and Haijun Wang*

Cite This: https://dx.doi.org/10.1021/acs.analchem.0c03311

Read Online

ACCESS | Metrics & More | Article Recommendations | Supporting Information

ABSTRACT: In this study, sulfur quantum dots (SQDs) with superior near-infrared electrochemiluminescence (ECL) performance were synthesized by the H_2O_2-assisted top-down approach. Through H_2O_2 etching, the size and dispersity of SQDs were adjusted, reducing the aggregation-caused quenching effect and obviously promoting the ECL performance. Using the obtained SQDs as an emitter, a super-sensitive ECL biosensor of microRNA-21 (miRNA-21) detection was constructed, which was based on an efficient DNA walking machine with triple-stranded DNA (tsDNA) nanostructures as tracks. Compared with the common single-stranded DNA or double-stranded DNA, the tsDNA nanostructures on the electrode interface could avert probe entanglement and decrease local overcrowding effects. The walking efficiency of the DNA walking machine was also improved and the signal-amplification efficacy was greatly enhanced, which was benefited from the fact that tsDNA nanostructures were highly rigid scaffolds and provided orderly tracks for the DNA walking machine to walk. Thus, the designed ECL biosensor demonstrated outstanding performance for miRNA-21 detection in the concentration range of 20 aM to 1 nM with a low detection limit of 6.67 aM. Remarkably, this work enriched the application of pure element quantum dots in the ECL field and offered a new avenue for ultra-sensitive detection in clinical and biochemical analysis.

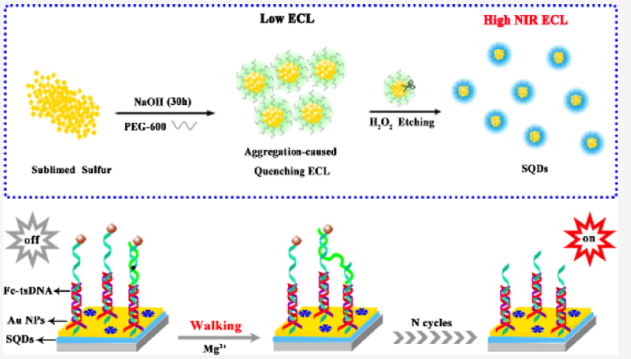

INTRODUCTION

Electrochemiluminescence (ECL) that combined the characteristics of electrochemical and chemiluminescence technology has shown advantages of low background, high selectivity, low detection limit, and wide response range.[1−3] In addition, ECL with near-infrared (NIR) emission has attracted much more interests in biomedical and diagnostic fields because of its excellent tissue penetration, negligible background interference, and low photochemical damage.[4,5] Quantum dots (QDs) have attracted much attention for their extremely impressive application in biological labeling, antimicrobial agents, light-emitting diodes, and displayers because of their quantum size effect, excellent magnetism, and good photoelectric properties.[6,7] However, heavy metal-based QDs (e.g., CdTe,[8] PbS,[9] and CdS[10]) have limited applications on account of potential toxicity and environmental hazards. Hence, in recent years, researchers have applied themselves to seeking for non-poisonous or heavy metal-free QDs, especially pure elemental QDs, such as carbon,[11−13] silicon,[14−16] phosphorus,[17−19] and sulfur,.[20−22] Among the reported pure elemental QDs, sulfur quantum dots (SQDs) have attracted increasing attention because of excellent aqueous dispersibility, low toxicity, outstanding chemical properties, and excellent biological activities.[23] However, to date, few literature studies about the ECL performance of SQDs were reported. Therefore, in this work, we attempted to explore the ECL of SQDs and its application in biosensors, especially for the near-infrared electrochemiluminescence (NIR ECL) performance affected by size.

Some fluorophores had bright emission in the solution state but had weak or no fluorescence after the aggregation of them, which was known as aggregation-caused quenching (ACQ) effect.[24] The reduction in the ACQ effect could improve the fluorescence intensity of luminescent materials and expand their application, which has become a popular research domain in recent years. According to previous literature,[21] it was found that the size of S dots could affect the fluorescence intensity. In this work, we tried to explore ECL performance by adjusting the size and dispersity of SQDs. It was found that the ACQ effect also obviously influenced the ECL performance of SQDs. S dots had weak ECL performance while SQDs obtained by

Received: August 4, 2020
Accepted: October 14, 2020

Scheme 1. Description Process of Biosensor Construction: (A) Synthesis of the SQDs, (B) DSN Enzyme-Assisted Target Cycling Amplification Process, and (C) Modification of the Electrode

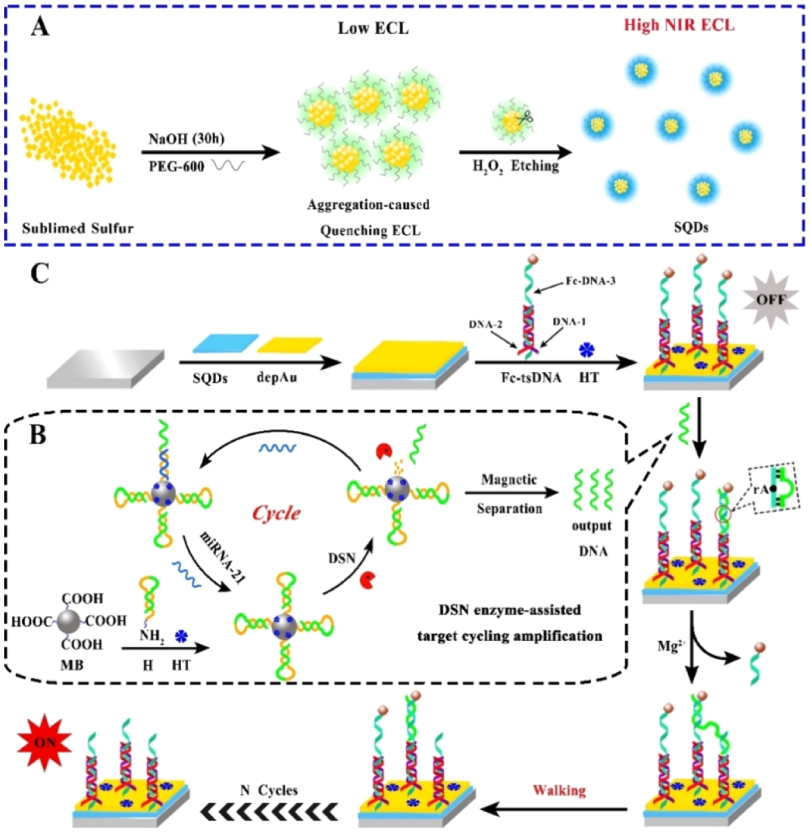

etching S dots with H_2O_2 showed high NIR ECL intensity. The reason was that H_2O_2 could change the size of the S dots and make them more dispersive, which weakened the ACQ effect and obviously improved the ECL performance.

MicroRNAs (miRNAs) were a kind of microcosmic and abundant noncoding RNAs, whose abnormal expression was related to many diseases, so the ultrasensitive detection of miRNAs was still in high demand.[25,26] For improving the detection sensitivity, nucleic acid amplification strategies were widely used, including strand displacement amplification (SDA),[27] catalytic hairpin assembly (CHA),[28] loop-mediated isothermal amplification (LAMP),[29] and so on. Meanwhile, the construction of the DNA walking machine was also an effective way to improve the detection sensitivity. Besides, in the solution,[30,31] the DNA walking machine could also be assembled on the electrode surface.[32−34] Also, single-stranded DNA (ssDNA) or double-stranded DNA (dsDNA) was usually used as tracks on the electrode surface to achieve signal amplification. However, both of them have the following problems: first, ssDNA or dsDNA was usually fixed on the electrode surface through the interaction of Au−S or Au−N bonds, which led to high modification cost and was easy to produce the by-product through the formation of the disulfide bond. Second, it was likely to cause probe entanglement and local overcrowding effects owing to the poor upright nature of ssDNA and dsDNA. Recently, new triple-stranded DNA (tsDNA) nanostructures have been reported in the literature.[35] They were composed of three ssDNAs modified with poly-adenine (polyA) blocks, which exhibited strong rigidity and uprightness. This might be attributed to the fact that polyA had a strong binding force with Au,[36,37] which could help us to form a stable triangular cone structure at the bottom of tsDNA. In this work, we tried to construct an efficient DNA walking machine with tsDNA nanostructures as tracks, which could greatly reduce entanglement and improve the walking efficiency, enhancing the signal amplification effect and obviously improving the sensitivity of the biosensor.

Herein, on the basis of S dots synthesized by the top-down approach, SQDs with superior NIR ECL performance and more excellent aqueous dispersibility could be obtained by adjusting the size to reduce the ACQ effect through H_2O_2 etching. Based on the SQDs with excellent ECL performance, an efficient DNA walking machine with tsDNA nanostructures as orbits was constructed in the fabrication of the ECL biosensor, which could effectively improve the walking efficiency of the DNA walking machine and detection sensitivity of miRNA-21. The process of material preparation and biosensor construction is shown in Scheme 1. First, S dots were synthesized by the hydrothermal method. Then, the particle size of S dots decreased and the dispersity was more uniform under the etching effect of H_2O_2, resulting in the formation of SQDs with excellent NIR ECL performance, which was shown in process A. The synthesized SQDs represented excellent water solubility, low toxicity, and excellent biocompatibility, and the preparation process was low-cost and easy to operate. Process B was the target cycling amplification process assisted by the duplex specific nuclease (DSN) enzyme. MiRNA-21 opened the hairpin H fixed in magnetic beads and the output DNA released with the cleavage action of the DSN enzyme. Meanwhile, miRNA-21 was also released and could enter the next cycle to open the next hairpin, which could realize circulation to achieve the

https://dx.doi.org/10.1021/acs.analchem.0c03311
Anal. Chem. XXXX, XXX, XXX−XXX

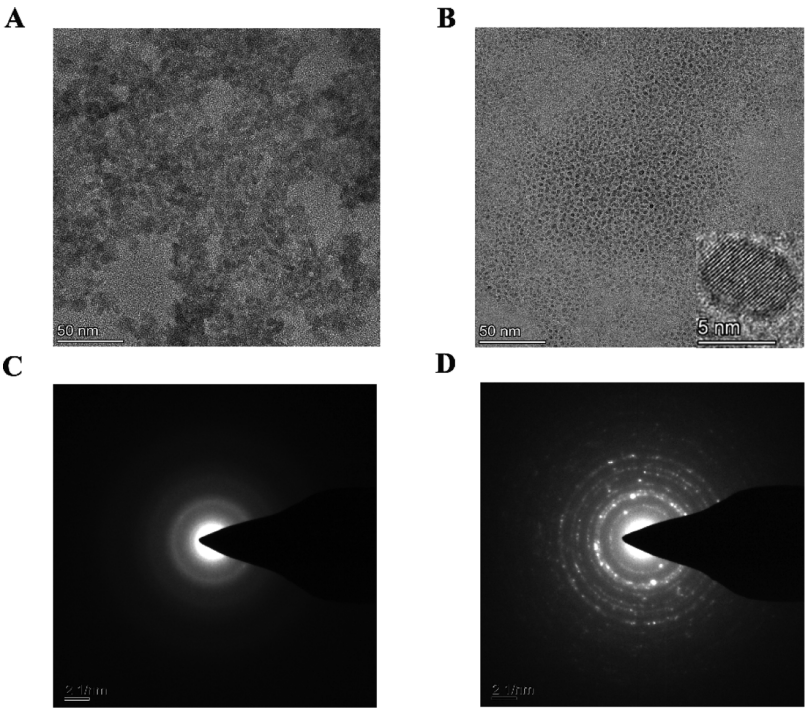

Figure 1. (A,B) TEM of the S dots and SQDs, respectively. Inset: Lattice fringe image. (C,D) SAED pattern of S dots and SQDs, respectively.

purpose of nucleic acid amplification. Then, masses of output DNA could be gained through magnetic separation. For the electrode modification in process C, SQDs dispersed in Nafion solution were immobilized on a glassy carbon electrode (GCE) to gain a considerable ECL signal (signal-on) in the presence of the coreagent $S_2O_8^{2-}$. Then, the tsDNA probe modified with ferrocene (Fc) was fixed on the electrode to provide DNA walker's walking orbits through the interaction of Au-ployA. Meanwhile, the ECL signal was significantly decreased because of the quenching effect of Fc for SQDs (signal-off). In addition, the output DNA hybridized, with the top of the tsDNA modified with the Mg^{2+} cleavage site. Based on the efficient DNA walking machine with tsDNA nanostructures as rails, a mass of partial DNA fragments modified with Fc were released under the cleavage action of Mg^{2+} and the recovered ECL signal was achieved (signal-on). Using SQDs with superior NIR ECL performance as an emitter and an efficient DNA walking machine based on tsDNA nanostructures as a signal amplifier, the biosensor had high sensitivity for miRNA-21.

EXPERIMENTAL SECTION

Synthesis of the SQDs/Nafion Composite Material. According to the reported literature studies,[21,22] S dots were synthesized by the top-down hydrothermal synthesis method, and the conversion of S dots to SQDs was completed with the aid of H_2O_2 etching. In brief, ultrapure water (50 mL), sublimated sulfur powder (1.4 g), NaOH (4.0 g), and polyethylene glycol 600 (3.0 mL) were mixed evenly in a three-neck flask first (one neck was inserted into a thermometer to indicate the temperature). At this time, the solution was layered. The upper layer was colorless and the lower layer was yellow powder. Then, the sublimated sulfur powder was dissolved in the abovementioned solution, leading to the color of the solution turn to yellow, orange, and finally to reddish brown with the extension of heating time (5−72 h) when the mixture was heated at 70 °C. Next, we could observe that a large number of bubbles emerged in the EP tube, and the solution would gradually change from reddish brown to colorless when the obtained reddish brown S dots were etched by H_2O_2. Finally, the prepared SQDs were mixed with Nafion solution to form the SQDs/Nafion composite material.

Preparation of Fc-Triple-Stranded DNA (Fc-tsDNA). First, the Fc-DNA-3 was obtained based on the following process: 5 mg of Fc-COOH was dispersed in phosphate-buffered solution (PBS, 0.1 M, pH = 7.4) which contained 0.01M *N*-hydroxy succinimide (NHS) and 0.04 M 1-ethyl-3-(3-dimethylaminopropyl) carbodiimide hydrochloride (EDC) and then the solution was stirred at 4 °C for 1 h to activate the carboxyl (COOH). Then, 100 μL of the abovementioned solution was mixed with 10 μL of DNA-3 (100 μM) and stored overnight at 4 °C to gain Fc-DNA-3 (9.1 μM).

Second, a dsDNA structure should be prepared as follows: 10 μL of DNA-1 (20 μM) in 0.1 M PBS (pH = 7.4) was added into the same concentration of DNA-2. Next, this mixture solution was heated at 95 °C for 5 min and then cooled to room temperature (RT), forming the hybrid double-stranded structure. Finally, 20 μL of 9.1 μM Fc-DNA-3 and 40 μL of 10 mM $MgCl_2$ (a final Mg^{2+} of 5 mM) were added into the solution, and the obtained solution was reacted for 12 h at 4 °C to form stable Fc-tsDNA and stored at 4 °C.

Target Cycling Amplification Process Assisted by the DSN Enzyme. With the assistance of the DSN enzyme, the circulation amplification process of the target is shown in Scheme 1B. First, carboxyl-MBs were activated for 2 h by 0.01 M NHS and 0.04 M EDC. Second, 20 μL of H (50 μM) was heated at 95 °C for 5 min and cooled to RT at 1 °C/min, followed by mixing 1 mL of the abovementioned carboxyl-MBs into the solution and stirring for 12 h. Then, MB@H was obtained through magnetic separation and then dispersed in PBS (500 μL, 0.10M, pH = 7.4). Next, nonspecific adsorption sites were blocked by 5 μL of hexanethiol (HT, 1 mM).

https://dx.doi.org/10.1021/acs.analchem.0c03311
Anal. Chem. XXXX, XXX, XXX−XXX

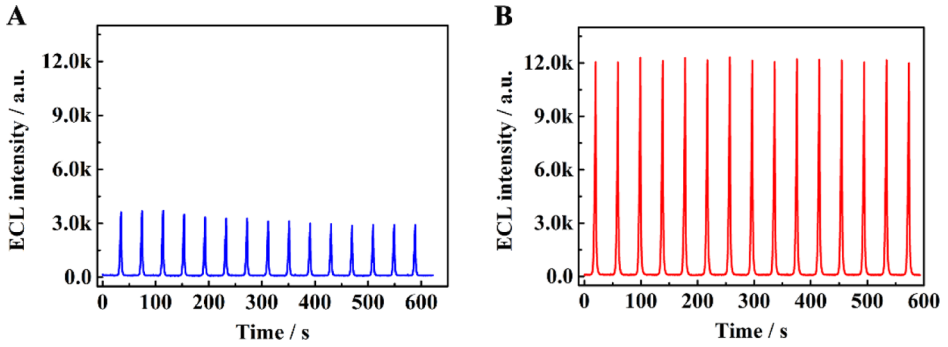

Figure 2. ECL intensity−time curve of S dots (A) and SQDs (B).

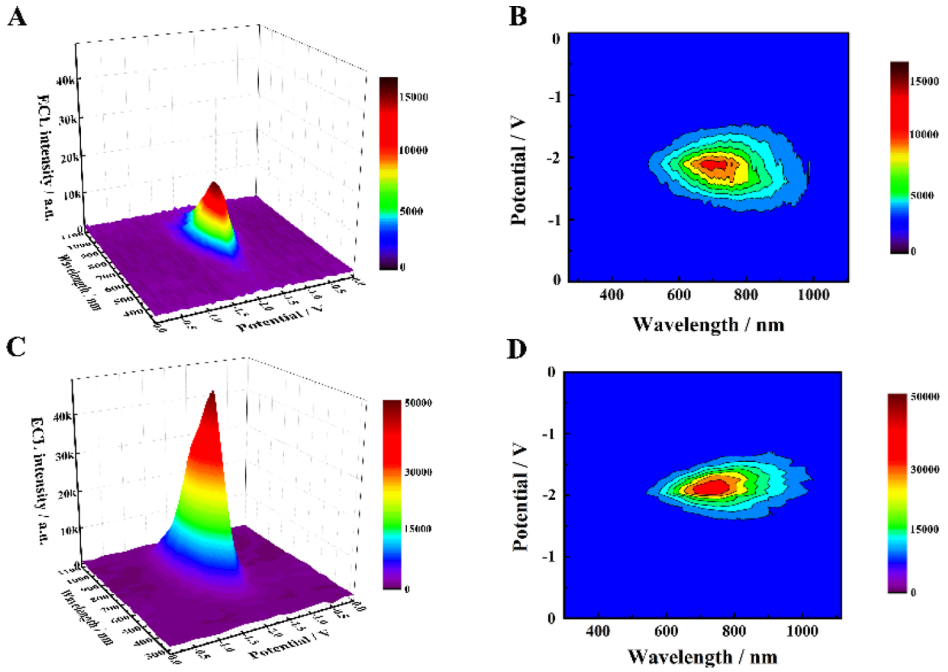

Figure 3. ECL spectra of S dots (A,B) and SQDs (C,D) via 3D surface image and 3D heat map image.

Subsequently, 1 × DSN master buffer, 1 U DSN, and different concentrations of miRNA-21 were mixed with 50 μL of Fe_3O_4@H and then heated at 60 °C for 70 min. After that, the mixture was inactivated by adding 5 μL of 2 × DSN stop solution and incubating at 60 °C for 5 min. Finally, the output DNA was separated by magnetic separation and used to hybridize with Fc-tsDNA on the electrode surface.

Fabrication of the ECL Biosensor. As shown in Scheme 1C, the GCE needs to be pretreated according to the methods reported in the literature[40] before using. For electrode modification, 15 μL of SQDs/Nafion solution was dropped on the electrode and dried at 37 °C first. Then, the SQDs/Nafion-modified GCE was immersed in $HAuCl_4$ solution (1%) for 15 s to obtain Au NPs/SQDs/Nafion/GCE and incubated with 10μL of Fc-tsDNA at RT for 16 h. Subsequently, the remaining active sites were blocked using HT (15 μL 1 mM) at RT for 1 h. Next, 10 μL of output DNA was dripped onto the upper electrode surface at 37 °C for 2 h to hybridize with Fc-tsDNA. Simultaneously, Mg^{2+} should be added to the abovementioned solution at the concentration of 10 mM to improve the hybridization efficiency. All the abovementioned steps should be rinsed with ultrapure water. The ECL measurements were performed in PBS (0.10 M, pH = 7.4) including 10 mM $S_2O_8^{2-}$ during the potential from 0 to −2.0 V at 100 mV/s.

RESULTS AND DISCUSSION

Morphology Characterization and ECL Intensity Comparison for Different Materials. We characterize the morphology of S dots and SQDs using transmission electron microscopy (TEM). As we can see from Figure 1A, S dots had poor monodispersibility and ambiguous boundary, which tended to aggregate into blocks before H_2O_2 etching. Meanwhile, S dots also showed a weak ECL intensity in the 0 to −2.0 V cycling scan (Figure 2A). However, it could be seen from Figure 1B that SQDs with uniform and smaller size distribution (3−5 nm), which was obtained by etching S dots with H_2O_2, showed a strong ECL response (Figure 2B). In addition, this could be caused by changes in particle size and dispersion after etching. Furthermore, the SQDs (Figure 1B) obtained by H_2O_2 etching had an ordered lattice typical than S dots (Figure 1C). Also, more TEM images of SQDs under different magnification are shown in Figure S3 of the Supporting Information. All of the above preliminarily proved that H_2O_2 etching was successful, and SQDs with better ECL performance were smaller and more dispersed than S dots.

https://dx.doi.org/10.1021/acs.analchem.0c03311
Anal. Chem. XXXX, XXX, XXX−XXX

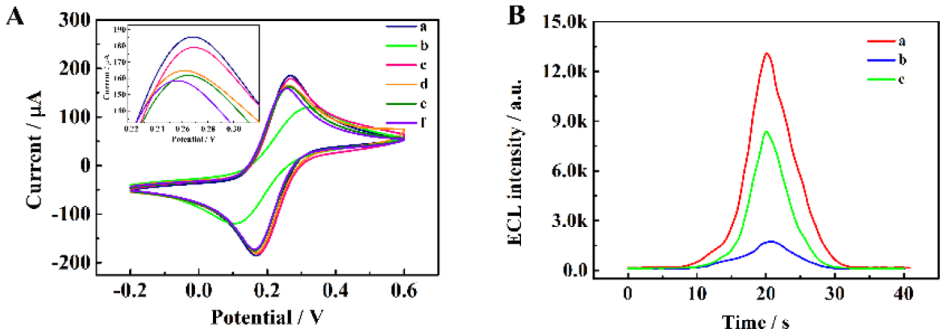

Figure 4. (A) CV analysis for different electrodes: bare GCE (a), GCE/Nafion/SQDs (b), GCE/Nafion/SQDs/Au NPs (c), GCE/Nafion/SQDs/Au NPs/Fc-tsDNA (d), GCE/Nafion/SQDs/Au NPs/Fc-tsDNA/HT (e), and GCE/Nafion/SQDs/Au NPs/Fc-tsDNA/HT/output DNA (f). Inset shows the enlarged partial CV curves. (B) ECL responses of the proposed biosensor fabrication process: GCE/Nafion/SQDs/Au NPs (a), GCE/Nafion/SQDs/Au NPs/Fc-tsDNA/HT (b), and GCE/Nafion/SQDs/Au NPs/Fc-tsDNA/HT/output DNA (c).

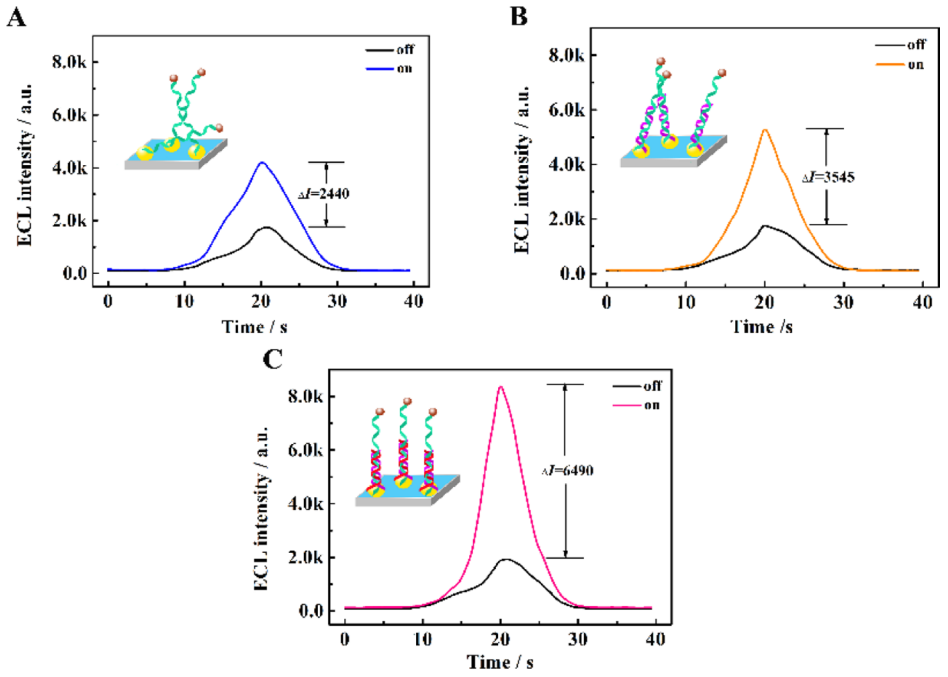

Figure 5. ECL responses of the biosensor using the DNA walking machine with different tracks as a signal amplifier: (A) DNA walking machine based on ssDNA, (B) DNA walking machine based on dsDNA, and (C) DNA walking machine based on tsDNA.

ECL Spectral Characteristics of Materials. In order to characterize S dots and SQDs, the photoluminescence (PL) spectra, PL quantum yields, UV−visible absorption spectra, and X-ray photoelectron spectroscopy (XPS) spectra of S dots and SQDs are presented in Figures S1, S2, and S4 of the Supporting Information. In addition, ECL spectra were also used to characterize S dots and SQDs. The ECL spectrum of S dots and SQDs was acquired using an electrochemiluminescence spectrophotometer. From Figure 3A,B, a notable ECL spectrum of S dots could be observed and a significant electrochemiluminescence emission peak at 685 nm was obtained. The ECL spectrum of SQDs is exhibited in Figure 3C,D, and an intense electrochemiluminescence (NIR ECL) emission peak at 730 nm was also obtained, which exhibited a distinct red shift ($\Delta\lambda$ = 45 nm) in comparison with that of S dots.

Cyclic Voltammetry and ECL Performance of the Designed Biosensor. We first used cyclic voltammetry (CV) to characterize the preparation process of this biosensor. From Figure 4A, a well-defined redox peak was exhibited on the bare GCE (curve a). When it was modified with SQDs/Nafion, the current decreased significantly owing to the hindrance of Nafion on electron transmission (curve b). When gold nanoparticles (Au NPs) were electrodeposited on the GCE, the increased redox current might result from the Au NPs that had excellent electrical conductivity (curve c). After incubating with Fc-tsDNA and HT in sequence, the redox current obviously decreased, suggesting that Fc-tsDNA and HT inhibited the transmission of electrons (curve d and e). When the output DNA was introduced, it could specially recognize tsDNA and then DNA-3 modified with Fc (electron media) was cleaved in the presence of Mg^{2+}, resulting in a slight decrease in the current (curve f). The abovementioned results meant that this biosensor has been successfully fabricated.

Moreover, ECL measurement was also carried out to confirm the feasibility of the sensing process. In Figure 4B, the Au NPs/SQDs/Nafion-modified electrode presented a significant ECL signal as SQDs had excellent ECL performance (signal-on, curve a). When Fc-tsDNA was modified, the sharp

https://dx.doi.org/10.1021/acs.analchem.0c03311
Anal. Chem. XXXX, XXX, XXX−XXX

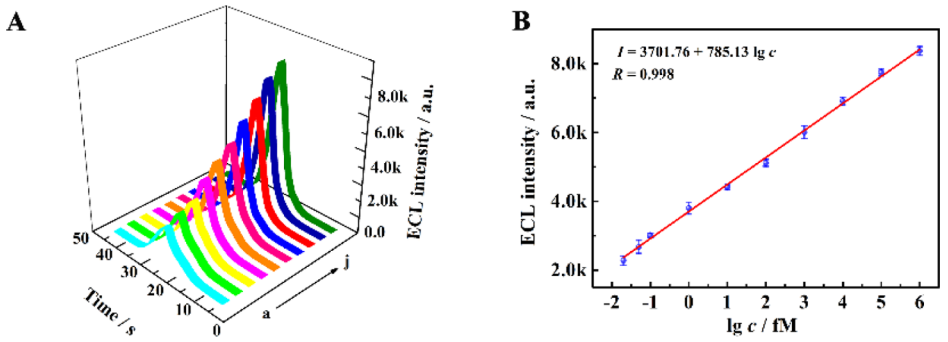

Figure 6. (A) ECL response at different miRNA-21 concentrations, from a to j: 2×10^{-2}, 5×10^{-2}, 10^{-1}, 1, 10, 10^2, 10^3, 10^4, 10^5, and 10^6 fM and (B) calibration curve for miRNA-21 detection.

decline in ECL intensity was observed because of the quenching effect of Fc (signal-off, curve b). The ECL intensity obviously recovered with the release of Fc (signal-off, curve c) after incubation with output DNA solution containing Mg^{2+}. The walking tracks provided by tsDNA nanostructures significantly improved the walking efficiency, which released a large amount of the Fc segment and dramatically enhanced the ECL response.

Walking Efficiency Comparison of the DNA Walking Machine with Different Tracks. To further demonstrate the advantages of the proposed biosensor, walking efficiency of the DNA walking machine based on the different orbitals was compared. Under the same experimental conditions, the changed ECL values (ΔI) which were obtained from the DNA walking machine with ssDNA as rails were 2440 a.u. (Figure 5A), while those of the DNA walking machine based on dsDNA were slightly enhanced to 3545 a.u. (Figure 5B). Most notably, ΔI of the proposed biosensor was significantly increased to 6490 a.u. when the DNA walking machine with tsDNA nanostructures as tracks was used (Figure 5C). The experimental phenomenon showed that the walking efficiency of the DNA walking machine with tsDNA nanostructures as tracks was much higher than that with others. This could be attributed to the fact that the tsDNA nanostructure was a highly rigid scaffold that provided an ordered track for the DNA walking machine, which could overcome the shortcoming of the ssDNA and dsDNA with probe entanglement and potential steric-hindrance effects.

ECL Analysis of this Proposed Biosensor. The biosensor was used for quantitative detection of miRNA-21 to study the performance under the optimum experimental conditions (Figure S6). As indicated from Figure 6, the corresponding stronger ECL responses were detected as the concentration of miRNA-21 was increased, indicating that there was a good linear relationship between the ECL signal and the logarithm of miRNA-21 concentration. The regression equation was $I = 3701.76 + 785.13 \log c (R = 0.998)$ in the range from 20 aM to 1 nM. In addition, the limit of detection (LOD) was as low as 6.67 aM. Moreover, compared with previous reports of existing miRNA-21 detection, this biosensor exhibited higher sensitivity and wide linear range, which proved that this biosensor had greater potential in bioassay (Table 1).

Other ECL Performance of This Proposed Biosensor. Reproducibility, selectivity, and stability that served as indicators of ECL performance have also been analyzed. As illustrated in Figure 7A, the biosensor incubated with different concentrations of miRNA-21 (10 fM and 1 nM) was investigated by 10 cycles of ECL measurements, the ECL responses have no distinct changes, and the relative standard deviation (RSD) was less than 5%, indicating that the biosensor had good stability. Then, as we can see from Figure S8 that the RSDs of inter-assay and intra-assay were estimated to be 2.36 % and 2.03 % for the miRNA-21 (1 nM) detection, respectively, indicating that this biosensor had good reproducibility.

Table 1. Comparison of Other Studies for miRNA-21 Detection

analytical method	linear range	LOD	reference
Electrochemical	0.1 fM to 0.1 pM	0.04 fM	38
Electrochemical	1 pM to 10 nM	1 pM	39
Fluorescence	1 pM to 2.5 nM	0.21 pM	40
ECL	0.5 fM to 10 pM	0.17 fM	41
ECL	50 aM to 50 pM	16 aM	42
ECL	20 aM to 1 nM	6.67 aM	present work

Furthermore, the ECL responses of the biosensor incubated with three interferents [miRNA-12 (100 pM), miRNA-141 (100 pM), and miRNA-155 (100 pM)] were investigated to evaluate the selectivity of miRNA-21 (1 pM). From the results shown in Figure 7B, the ECL responses of the interferents (miRNA-155, miRNA-141, and miRNA-122) showed little fluctuations compared with the blank group, while the ECL intensity was significantly enhanced in the presence of miRNA-21 (1 pM). The abovementioned results proved that the proposed biosensor had excellent selectivity for miRNA-21. Therefore, this biosensor had great potential in biological applications because of its high stability, reproducibility, and specificity.

Application. To test the feasibility of this biosensor in the detection of miRNA-21 in actual samples, we specifically analyzed the ECL responses in lysates of MCF-7 and HeLa. As presented in Figure 8, the ECL signal significantly enhanced as MCF-7 cell lysate concentrations increased, suggesting that miRNA-21 was highly expressed in MCF-7 cells, while the biosensor incubated with HeLa cell lysate displayed a slightly enhanced ECL intensity compared to that of the MCF-7 cell lysate, speculating that miRNA-21 was relatively less expressed in HeLa cells. To verify the accuracy of the method, the same samples were also measured using a commercial kit based on real-time quantitative reverse transcription polymerase chain reaction (qRT-PCR) (see Figure S10). The detection of the proposed biosensor was in good agreement with the qRT-PCR method, and the sensitivity of this biosensor was higher than that of qRT-PCR method.

https://dx.doi.org/10.1021/acs.analchem.0c03311
Anal. Chem. XXXX, XXX, XXX−XXX

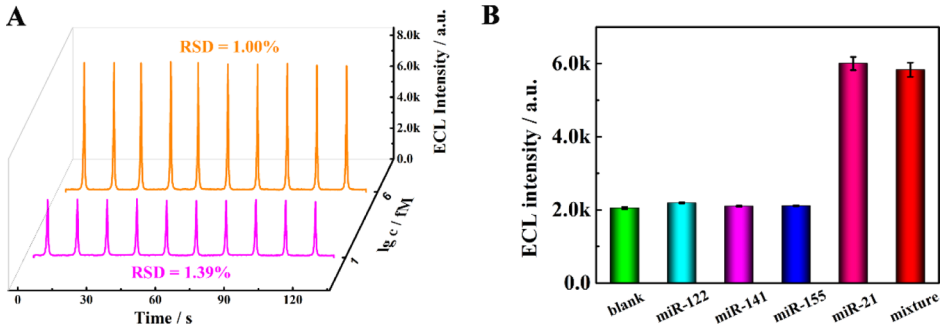

Figure 7. (A) ECL stability of this biosensor under 10 scanning cycles. (B) Selectivity of the proposed biosensor with different targets.

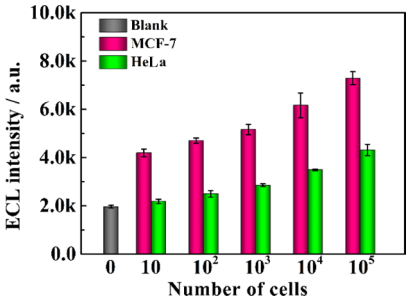

Figure 8. ECL response of the proposed biosensor with different numbers of MCF-7 and HeLa cells.

All the abovementioned results were consistent with previous reports,[39,41] which indicated that this biosensor had good application potential for sensitive detection of miRNA in cancer cells.

CONCLUSIONS

In summary, we used the H_2O_2-assisted top-down approach to synthesize SQDs with superior NIR-ECL performance and constructed an ultrasensitive ECL biosensor for miRNA-21 detection which used SQDs as emitters and an efficient DNA walking machine based on tsDNA nanostructures for signal amplification. First, SQDs with excellent NIR ECL performance were synthesized through etching S dots with H_2O_2, which could obviously reduce the ACQ effect. Second, the sensitivity of the target miRNA-21 could be enhanced through the DSN enzyme-assisted target cycling amplification strategy. Third, tsDNA nanostructures serving as walking tracks overcame the shortcoming of the ssDNA and dsDNA with probe entanglement and potential steric-hindrance effects. Finally, an efficient DNA walking machine with tsDNA nanostructures as tracks could greatly improve walking efficiency to achieve ECL signal recovery. The proposed "off-on" ECL biosensor had outstanding selectivity and stability and could be available for ultrasensitive detection of miRNA-21 with good performance. Considering these advantages, the proposed biosensor using SQDs with superior NIR ECL performance and the highly efficient DNA walking machine with tsDNA as tracks exhibited great potential in biomedical detection and early clinical diagnosis.

ASSOCIATED CONTENT

Supporting Information

The Supporting Information is available free of charge at https://pubs.acs.org/doi/10.1021/acs.analchem.0c03311.

Reagents and materials, instruments, fluorescence spectral, PL quantum yields (QYs) and UV−visible absorption spectra characterization of materials, TEM images of SQDs, XPS of S dots and SQDs, normalized ECL spectra of $S_2O_8^{2-}$, optimal conditions of the material, characterization of the tsDNA, reproducibility of the proposed biosensor, and quantitative real-time fluorescence detecting microRNA-21 in the real sample (PDF)

AUTHOR INFORMATION

Corresponding Authors

Ruo Yuan − *Key Laboratory of Luminescence Analysis and Molecular Sensing (Southwest University), Ministry of Education, College of Chemistry and Chemical Engineering, Southwest University, Chongqing 400715, PR China;* orcid.org/0000-0003-3664-6236; Phone: +86-23-68252277; Email: yuanruo@swu.edu.cn; Fax: +86-23-68253172

Haijun Wang − *Key Laboratory of Luminescence Analysis and Molecular Sensing (Southwest University), Ministry of Education, College of Chemistry and Chemical Engineering, Southwest University, Chongqing 400715, PR China;* Email: hjwang@swu.edu.cn

Authors

Linlei Liu − *Key Laboratory of Luminescence Analysis and Molecular Sensing (Southwest University), Ministry of Education, College of Chemistry and Chemical Engineering, Southwest University, Chongqing 400715, PR China*

Yue Zhang − *Key Laboratory of Luminescence Analysis and Molecular Sensing (Southwest University), Ministry of Education, College of Chemistry and Chemical Engineering, Southwest University, Chongqing 400715, PR China*

Complete contact information is available at: https://pubs.acs.org/10.1021/acs.analchem.0c03311

Notes

The authors declare no competing financial interest.

ACKNOWLEDGMENTS

This work was financially supported by the National Natural Science Foundation (NNSF) of China (21804110), the Venture & Innovation Support Program for Chongqing Overseas Returnees (cx2019059), and the Fundamental Research Funds for the Central Universities (SWU019017).

REFERENCES

(1) Qi, H.; Zhang, C. *Anal. Chem.* **2020**, *92*, 524−534.

https://dx.doi.org/10.1021/acs.analchem.0c03311
Anal. Chem. XXXX, XXX, XXX−XXX

(2) Chen, Y.; Zhou, S.; Li, L.; Zhu, J.-j. *Nano Today* **2017**, *12*, 98−115.
(3) Zhao, G.; Wang, Y.; Li, X.; Yue, Q.; Dong, X.; Du, B.; Cao, W. *Anal. Chem.* **2019**, *91*, 1989−1996.
(4) Voci, S.; Goudeau, B.; Valenti, G.; Lesch, A.; Jović, M.; Rapino, S.; Paolucci, F.; Arbault, S.; Sojic, N. *J. Am. Chem. Soc.* **2018**, *140*, 14753−14760.
(5) Liu, J.-L.; Zhang, J.-Q.; Tang, Z.-L.; Zhuo, Y.; Chai, Y.-Q.; Yuan, R. *Chem. Sci.* **2019**, *10*, 4497−4501.
(6) Zhao, T.; Goodwin, E. D.; Guo, J.; Wang, H.; Diroll, B. T.; Murray, C. B.; Kagan, C. R. *ACS Nano* **2016**, *10*, 9267−9273.
(7) Castan, A.; Kim, H.-M.; Jang, J. *ACS Appl. Mater. Interfaces* **2014**, *6*, 2508−2515.
(8) Jie, G.; Li, C.; Zhao, Y.; Kuang, Q.; Niu, S. *ACS Appl. Nano Mater.* **2019**, *2*, 4637−4645.
(9) Hesari, M.; Swanick, K. N.; Lu, J.-S.; Whyte, R.; Wang, S.; Ding, Z. *J. Am. Chem. Soc.* **2015**, *137*, 11266−11269.
(10) Zhang, Y.; Xiao, J.-Y.; Zhu, Y.; Tian, L.-J.; Wang, W.-K.; Zhu, T.-T.; Li, W.-W.; Yu, H.-Q. *Anal. Chem.* **2020**, *92*, 3990−3997.
(11) Zhou, Y.; Yang, S.; Fan, D.; Reilly, J.; Zhang, H.; Yao, W.; Huang, J. *ACS Appl. Nano Mater.* **2019**, *2*, 1027−1032.
(12) Jiang, X.; Qin, D.; Mo, G.; Feng, J.; Zheng, X.; Deng, B. *Anal. Chem.* **2019**, *91*, 11455−11460.
(13) Fan, Q.; Li, J.; Zhu, Y.; Yang, Z.; Shen, T.; Guo, Y.; Wang, L.; Mei, T.; Wang, J.; Wang, X. *ACS Appl. Mater. Interfaces* **2020**, *12*, 4797−4803.
(14) He, Y.; Zhong, Y. L.; Peng, F.; Wei, X. P.; Su, Y. Y.; Lu, Y. M.; Su, S.; Gu, W.; Liao, L. S.; Lee, S. T. *J. Am. Chem. Soc.* **2011**, *133*, 14192−14195.
(15) Bergren, M. R.; Palomaki, P. K. B.; Neale, N. R.; Furtak, T. E.; Beard, M. C. *ACS Nano* **2016**, *10*, 2316−2323.
(16) Noiri, A.; Takeda, K.; Yoneda, J.; Nakajima, T.; Kodera, T.; Tarucha, S. *Nano Lett.* **2020**, *20*, 947−952.
(17) Niu, X.; Li, Y.; Shu, H.; Wang, J. *J. Phys. Chem. Lett.* **2016**, *7*, 370−375.
(18) Sun, Z.; Xie, H.; Tang, S.; Yu, X.-F.; Guo, Z.; Shao, J.; Zhang, H.; Huang, H.; Wang, H.; Chu, P. K. *Angew. Chem., Int. Ed.* **2015**, *54*, 11526−11530.
(19) Ren, X.; Yang, X.; Xie, G.; Luo, J. *ACS Appl. Nano Mater.* **2020**, *3*, 4799−4809.
(20) Wang, Z.; Zhang, C.; Wang, H.; Xiong, Y.; Yang, X.; Shi, Y. e.; Rogach, A. L. *Angew. Chem., Int. Ed.* **2020**, *59*, 9997−10002.
(21) Shen, L.; Wang, H.; Liu, S.; Bai, Z.; Zhang, S.; Zhang, X.; Zhang, C. *J. Am. Chem. Soc.* **2018**, *140*, 7878−7884.
(22) Wang, H.; Wang, Z.; Xiong, Y.; Kershaw, S. V.; Li, T.; Wang, Y.; Zhai, Y.; Rogach, A. L. *Angew. Chem., Int. Ed.* **2019**, *58*, 7040−7044.
(23) Shi, Y.-e.; Zhang, P.; Yang, D.; Wang, Z. *Chem. Commun.* **2020**, *56*, 10982.
(24) Arshad, F.; Sk, M. P. *ACS Appl. Nano Mater.* **2020**, *3*, 3044−3049.
(25) Chen, K.; Huang, Q.; Fu, T.; Ke, G.; Zhao, Z.; Zhang, X.; Tan, W. *Anal. Chem.* **2020**, *92*, 7404−7408.
(26) Hou, T.; Li, W.; Liu, X.; Li, F. *Anal. Chem.* **2015**, *87*, 11368−11374.
(27) Huang, Z.; Chen, J.; Luo, Z.; Wang, X.; Duan, Y. *Anal. Chem.* **2019**, *91*, 4806−4813.
(28) Yang, X.-J.; Cui, M.-R.; Li, X.-L.; Chen, H.-Y.; Xu, J.-J. *Chem. Commun.* **2020**, *56*, 2135−2138.
(29) Varona, M.; Anderson, J. L. *Anal. Chem.* **2019**, *91*, 6991−6995.
(30) Yang, P.; Li, Y.; Mason, S. D.; Chen, F.; Chen, J.; Zhou, R.; Liu, J.; Hou, X.; Li, F. *Anal. Chem.* **2020**, *92*, 3220−3227.
(31) Oishi, M.; Saito, K. *ACS Nano* **2020**, *14*, 3477−3489.
(32) Yang, X.; Shi, D.; Zhu, S.; Wang, B.; Zhang, X.; Wang, G. *ACS Sens.* **2018**, *3*, 1368−1375.
(33) Chen, J.-X.; Zhuo, Y.; Peng, X.; Chai, Y.-Q.; Yuan, R.; Liang, W.-B. *Anal. Chem.* **2019**, *91*, 14125−14132.
(34) Ge, J.; Zhao, Y.; Gao, X.; Li, H.; Jie, G. *Anal. Chem.* **2019**, *91*, 14117−14124.
(35) Lu, L.; Wang, J.; Miao, W.; Wang, X.; Guo, G. *Anal. Chem.* **2019**, *91*, 1452−1459.
(36) Pei, H.; Li, F.; Wan, Y.; Wei, M.; Liu, H.; Su, Y.; Chen, N.; Huang, Q.; Fan, C. *J. Am. Chem. Soc.* **2012**, *134*, 11876−11879.
(37) Yang, K.; Wang, H.; Ma, N.; Zeng, M.; Luo, H.; He, D. *ACS Appl. Mater. Interfaces* **2018**, *10*, 44546−44553.
(38) Lu, J.; Wang, J.; Hu, X.; Gyimah, E.; Yakubu, S.; Wang, K.; Wu, X.; Zhang, Z. *Anal. Chem.* **2019**, *91*, 7353−7359.
(39) Zhu, L.; Miao, M.; Shao, X.; Du, Z.; Huang, K.; Luo, Y.; Xu, W. *Anal. Chem.* **2019**, *91*, 14992−14999.
(40) Peng, X.; Wen, Z. B.; Yang, P.; Chai, Y. Q.; Liang, W. B.; Yuan, R. *Anal. Chem.* **2019**, *91*, 14920−14926.
(41) Peng, L.; Yuan, Y.; Fu, X.; Fu, A.; Zhang, P.; Chai, Y.; Gan, X.; Yuan, R. *Anal. Chem.* **2019**, *91*, 3239−3245.
(42) Gao, H.; Zhang, J.; Liu, Y.; Tu, W.; Wei, T.; Dai, Z. *Anal. Chem.* **2019**, *91*, 12038−12045.

https://dx.doi.org/10.1021/acs.analchem.0c03311
Anal. Chem. XXXX, XXX, XXX−XXX